ELSEVIER

Chemical Engineering Journal 82 (2001) 117–129

Chemical Engineering Journal

www.elsevier.com/locate/cej

Electrochemical chlorine absorption in cyclone membrane reactor: analysis of reaction mechanism and transport phenomena

K. Sundmacher [a,b,*], T. Schultz [a]

[a] *Max-Planck-Institut für Dynamik komplexer technischer Systeme, Leipziger Straße 44, ZENIT-Building, D-39120 Magdeburg, Germany*
[b] *Lehrstuhl für Systemverfahrenstechnik, Institut für Verfahrenstechnik, Otto-von-Guericke-Universität Magdeburg, Universitätsplatz 2, D-39106 Magdeburg, Germany*

Received 16 May 2000; accepted 24 October 2000

Abstract

A new reactive separation process is presented and analyzed which is based on simultaneous, dispersionless gas–liquid absorption and electrochemical reaction in the pore structure of electrically conductive membranes. As a model process of technical and environmental relevance, the electrochemical absorption of chlorine waste gases in hydrochloric acid is studied, both experimentally and theoretically. The membranes were manufactured from porous carbon black particles by rolling agglomeration. The reaction mechanisms and mass transport phenomena within these membranes were investigated in a novel cyclone flow reactor. With this membrane reactor, a series of experiments was carried out under control of membrane electrode potential using chlorine–nitrogen gas mixtures (1000 ppm Cl_2). A model-based analysis of experimental data reveals the electrochemical reaction microkinetics to follow the Volmer–Heyrovsky mechanism. Mass transport was found to be dominated by Knudsen diffusion in the membrane micropores.

Keywords: Absorption; Membrane reactor; Electrochemical reaction; Chlorine; Mikrokinetics; Cyclone flow reactor

1. Introduction

Electrochemical absorbers are multi-phase reactors in which gaseous components are uptaken in a liquid electrolyte and, by charge transfer in contact with a solid electrode surface, are converted to ionic species. Electrochemical absorption processes are environmentally friendly and offer several advantages compared to conventional chemical absorption processes [1,2]. The driving force for gas–liquid mass transfer is increased dramatically by the electrochemical reaction without using any chemical washing substances. Moreover, the absorption process can be controlled easily via adjustment of the electrode potential.

In this work, the application of an electrochemical absorption process will be discussed for the removal of chlorine from a process waste gas stream, e.g. from the AEROSIL process [3]. There, the chlorine concentration in the effluent is typically around 1000 ppm, while the German environment protection legislation allows a maximum content of 1 mg m_N^{-3} (0.3 ppm) for waste gases emitted into the atmosphere. As a very efficient reactor to carry out chlorine absorption, a gas–liquid membrane reactor is applied. The membrane used is a porous gas-diffusion electrode (GDE) [6].

As an important step to design such a reactor, single membranes have to be characterized under well-defined flow conditions on either side of the membrane. This is necessary because of the influence of external mass transport phenomena in the boundary layers on both sides of the membrane, due to the low concentration of the reactant chlorine. For this purpose, a novel electrochemical flow cell was developed and was characterized with respect to mass transport through the boundary layers at the external membrane surface [4]. These mass transfer studies were based on limiting current measurements using simple, well-understood electrochemical reaction, i.e. the oxidation of ferricyanide(II) ions on the surface of a nonporous graphite electrode membrane. The mass transfer coefficients were casted into a dimensionless data correlation, i.e. a Sherwood function. With this function, external mass transfer resistances through the boundary layers are estimated for the chlorine reduction process at porous electrodes. This allows to identify the internal diffusion coefficients and microkinetic reaction parameters from

Abbreviations: GDE, gas-diffusion electrode; NHE, normal hydrogen electrode

*Corresponding author. Tel.: +49-391-6718704; fax: +49-391-6711245.
E-mail address: kai.sundmacher@vst.uni-magdeburg.de (K. Sundmacher).

1385-8947/01/$ – see front matter
PII: S1385-8947(00)00361-2

Nomenclature

Symbols

a_i	liquid phase activity of component i
ai_0	exchange current density related to membrane volume ($A\,m^{-3}$)
B	parameter group, Eq. (37)
$Bi_m^{G/L}$	Biot number for mass transfer on gas or liquid side, see Table 1
c_i	molar concentration of component i in liquid phase ($mol\,m^{-3}$)
c_i^{*L}	dimensionless molar concentration of component i in liquid bulk
d	membrane thickness (m)
d^*	dimensionless thickness of flooded layer, see Table 1
d^{FL}	thickness of flooded layer (m)
d^{GL}	thickness of the gas-filled layer in membrane (m)
$d_{p,eq}$	pore equivalent diameter (m)
D^*	dimensionless ratio of mass transfer resistances in gas-filled layer and in flooded membrane layer, see Table 1
$D_{eff,i}$	effective diffusion coefficient of component i in pore system ($m^2\,s^{-1}$)
D_i	diffusion coefficients of component i ($m^2\,s^{-1}$)
F	Faraday's constant ($96485\,C\,mol^{-1}$)
Ha	Hatta number, see Table 1
i_{eff}	effective current density related to cross sectional area ($A\,m^{-2}$)
i_{eff}^*	dimensionless effective current density, see Table 1
i_{lim}	limiting current density ($A\,m^{-2}$)
i_{lim}^*	dimensionless limiting current density
i_{max}	maximum current density related to cross sectional area ($A\,m^{-2}$)
i_n	local current density related to inner electrode surface ($A\,m^{-2}$)
i_n^*	dimensionless local current density, see Table 1
i_0	exchange current density ($A\,m^{-2}$)
K_V	equilibrium constant of Volmer reaction
$K_{V,0}$	equilibrium constant of Volmer reaction at $i_n = 0$
$k_{a/c}$	reaction rate constants for anodic and cathodic reaction
$k_i^{G/L}$	mass transfer coefficient of component i on gas/liquid side
M_i	molecular weight of component i ($kg\,mol^{-1}$)
n	number of transferred electrons; for chlorine reduction, $n = 2$
p	total pressure (Pa)
p_i^G	partial pressure of component i in gas phase (Pa)
r^*	dimensionless spacial coordinate, see Table 1
R	universal gas constant ($J\,mol^{-1}\,K^{-1}$)
Re	Reynolds number, Eq. (5)
Sc	Schmidt number, Eq. (6)
Sh	Sherwood number, Eq. (4)
T	temperature (K, °C)
U	electrode potential versus NHE (V)
U^θ	thermodynamic equilibrium electrode potential versus NHE (V) (for chlorine reduction, $U^\theta = 1.269\,V$ at 1000 ppm Cl_2 and $c_{Cl^-}^L = 1\,mol\,dm^{-3}$)
$V^{G/L}$	gas and liquid flow rate ($m^3\,s^{-1}$)

Greek symbols

$\alpha_{a/c}$	anodic and cathodic charge transfer coefficient
β_s	symmetry factors in Eqs. (15) and (16)
δ	thickness of hydrodynamic boundary layer (m)
ε	total porosity of GDE
ϕ	electrostatic potential (V)
η	electrode overpotential (V), Eq. (25)
μ	dynamic viscosity of fluid ($Pa\,s^{-1}$)
ν_i	stoichiometric coefficient of component i (for chlorine, value is -1)
Θ_i	fraction of inner surface covered by component i
ρ	mass density of fluid ($kg\,m^{-3}$)
ω	angular velocity (s^{-1})

Subscripts

a	anodic reaction
c	cathodic reaction
eff	effective quantity, i.e. related to cross sectional area
H	Heyrovsky reaction
i	index of components
lim	at limiting current conditions
max	maximum
ref	with respect to reference mixture
V	Volmer reaction

Superscripts

e	at gas–liquid equilibrium
FL	flooded layer of porous membrane
G	gas bulk
GL	gas-filled layer of porous membrane
L	liquid bulk
S	solid phase
*	dimensionless quantity
θ	standard conditions (ideal gas at $p^\theta = 0.1$ MPa, ideal solution with ion molality of $m^\theta = 1\,mol\,kg^{-1}$ water)

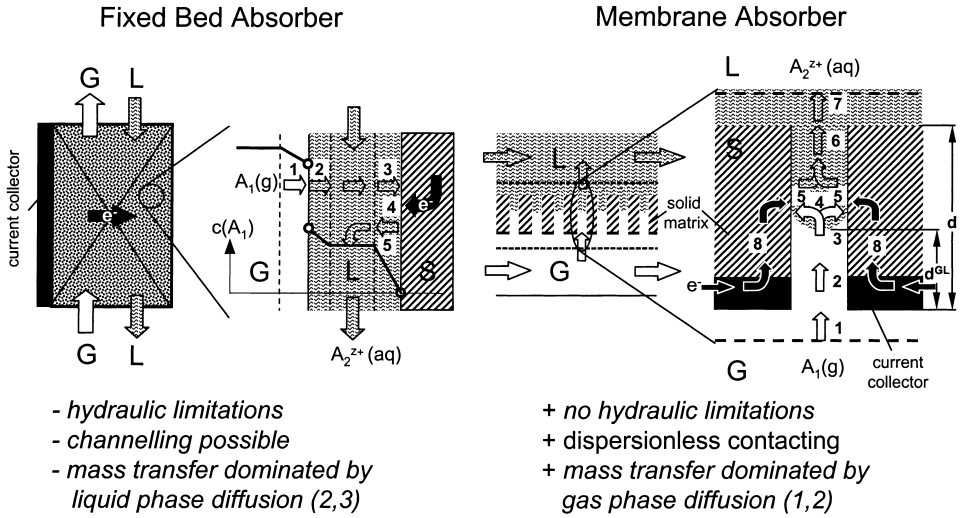

Fig. 1. Reactor concepts for electrochemical gas absorption and relevant mass transport phenomena (G: gas phase, L: liquid phase, S: solid phase); left: classical countercurrent fixed bed reactor; right: membrane reactor.

macrokinetic measurements of chlorine reduction at porous electrode membranes. In Section 2, the principle of an electrochemical membrane reactor is illustrated and is compared to classical fixed bed absorber.

2. Principles of electrochemical gas absorption

The general requirements for an electrochemical gas absorption are a thorough contact between the gas phase and the absorbing liquid phase on one hand (to transfer the reactant from the gas phase to the liquid phase), and a thorough contact between the liquid phase and the solid electrode on the other hand (to realize an electric current through the system). These requirements can be met by using either a fixed or fluidized bed of particles forming the electrode [5], or by using a GDE in a membrane reactor [4]. Both principles are described schematically in Fig. 1.

In the fixed bed absorber (Fig. 1, left), as well as in fluidized bed absorbers, the gaseous component $A_1(g)$ has to overcome first the mass transport resistances in the external gas film (step 1), before it is absorbed in the liquid phase. After that, two additional mass transport resistances in the liquid phase have to be overcome: in the liquid film at the gas–liquid interface (step 2) and in the liquid–solid film attached to the solid surface (step 3). Finally, the electrochemical reaction takes place (step 4), followed by film diffusion of the product $A_2(aq)$ into the liquid bulk (step 4).

In case of a membrane reactor (Fig. 1: right), the gas and the liquid phase are contacted within the pore structure of the membrane. The gaseous component $A_1(g)$ has to overcome the mass transport resistances in the external gas film (step 1) and in the gas-filled pore volume (step 2), before it is absorbed in the liquid phase (step 3). Here, in the liquid-filled pore volume, another diffusional mass transport resistance has to be overcome (step 4), before finally the electrochemical reaction takes place to form the ionic product $A_2(aq)$ (step 5). The latter is then transported to the liquid bulk via liquid-phase pore diffusion (step 6) and external film diffusion (step 7). The electrons e^- participating in the charge transfer reaction are transported through the solid electrode matrix by Ohmic conduction (step 8).

The main advantages of the membrane reactor concept are the dispersionless gas–liquid contacting and the possibility to apply any ratio of gas flow to liquid flow without hydraulic limitations. In addition, in case of an instantaneous electrochemical reaction, the absorbed reactant $A_1(g)$ will be totally converted at the gas–liquid interface and, therefore, the gas absorption rate will be only limited by gas-phase diffusion (Fig. 1: right, steps 1 and 2). In contrast, the absorption rate of a classical countercurrent fixed bed absorber will be dominated by diffusional transport phenomena in the liquid trickling down along the electrode (Fig. 1: left, steps 3 and 4). Due to the fact that gas phase transport will be much faster than liquid phase transport, one can expect that the membrane absorber concept leads to much higher absorption rates and a more compact reactor design. Of course, this is true only if membranes are thin enough and have a sufficient total porosity [6].

In order to demonstrate the feasibility of the described membrane reactor concept, it is reasonable to investigate first the mass transport and electrochemical reaction processes at single porous electrode membranes under well defined flow conditions without any concentration gradients along the membrane surface, i.e. in a parametrically concentrated flow system. Since no reliable flow system for the investigation of gas–liquid membranes was available so far, a novel cyclone reactor was developed which is explained in Section 3.

3. Cyclone flow reactor for membrane characterization

In classical electrochemistry, rotating disc electrodes (RDE) are used to investigate reaction and transport phenomena at planar electrodes. By controlled rotation of the electrode in a stationary fluid, a well defined flow field at the electrode surface is generated. The rotational flow field leads to a hydrodynamic boundary layer of constant thickness δ_{RDE} over the electrode surface:

$$\delta_{\mathrm{RDE}} = 4\left(\frac{\mu}{\rho\omega}\right)^{1/2} \tag{1}$$

In Eq. (1), μ denotes the dynamic viscosity of the fluid, ρ its mass density and ω the angular velocity of the rotation. Unfortunately, the RDE is not directly applicable to the characterization of a porous GDE membrane in whose pore structure a gaseous reactant and a liquid electrolyte are brought into contact from opposite sides. Therefore, a special design for a novel electrochemical cell was needed.

The basic idea of the novel flow cell was to achieve a similar vortex-type flow field to that in the RDE assembly, but to keep the membrane electrode fixed while the fluids on both sides of the membrane are set into rotational motion. A vortex flow with constant angular velocity ω over an infinite surface as shown in Fig. 2 has been the subject of extensive theoretical investigation [7]. It is qualitatively similar to that of a rotating disc electrode and the thickness of the hydrodynamic boundary layer was found to be

$$\delta_{\mathrm{vortex}} = 8\left(\frac{\mu}{\rho\omega}\right)^{1/2} \tag{2}$$

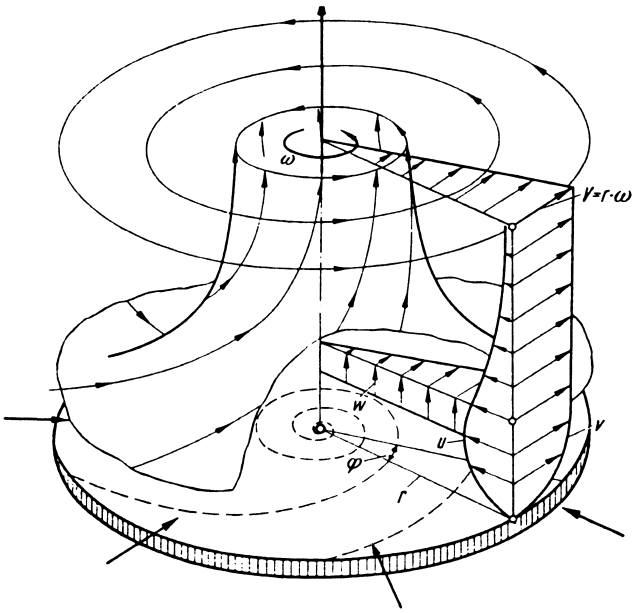

Fig. 2. Vortex flow field above an infinitely extended, fixed surface (adopted from [7]).

which is exactly twice the value found for the rotating disc assembly [8,9].

As the cell has to be used to examine systems with poisonous (e.g. chlorine) and/or hazardous components (e.g. hydrochloric acid), a construction using rotors, stirrers, etc. would lead to severe problems in preventing leakage. Therefore, it was decided to generate the desired vortex flow field by using the cyclone principle as widely used in mechanical engineering applications. Here, the fluid is set into rotation forced by a special geometry. The fluid compartment has a conical shape, converging to the electrode. The fluid is tangentially introduced at the upper edge of the cone and follows a circular path towards the cone end. For reason of continuity, the fluid rises in the middle of the cone and is removed by an inner tube.

In order to achieve such a vortex flow field on both sides of a GDE membrane, two cyclones are combined, with the membrane in-between them (see Fig. 3). The upper cyclone is providing for the liquid phase, while the lower cyclone is providing for the gas phase. Both sides can be operated independently. The overall experimental set-up is shown schematically in Fig. 4.

External mass transfer from the bulk phase in each cyclone through the boundary layer towards the membrane surface was characterized by using a simple, electrochemical model reaction system, i.e. the oxidation of ferricyanide(II)

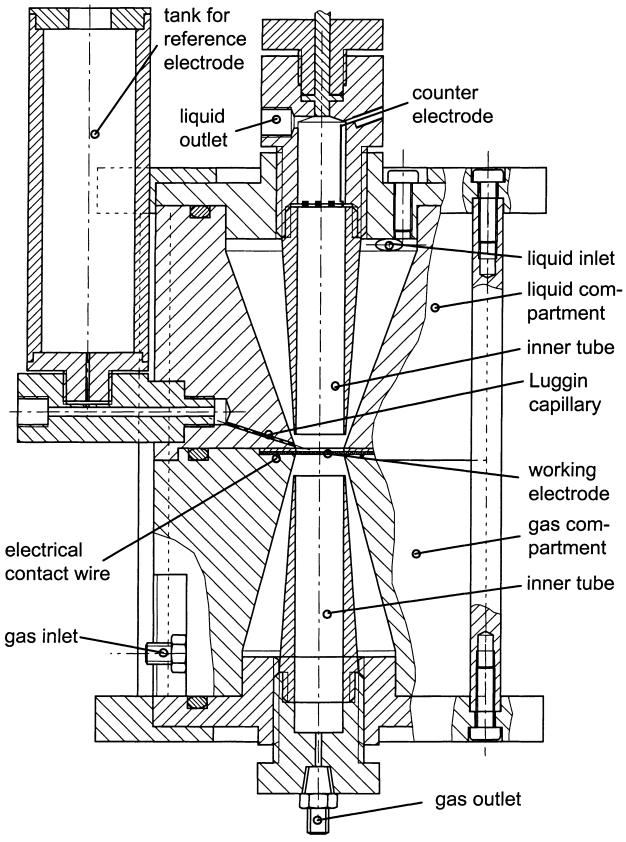

Fig. 3. Design of cyclone flow reactor.

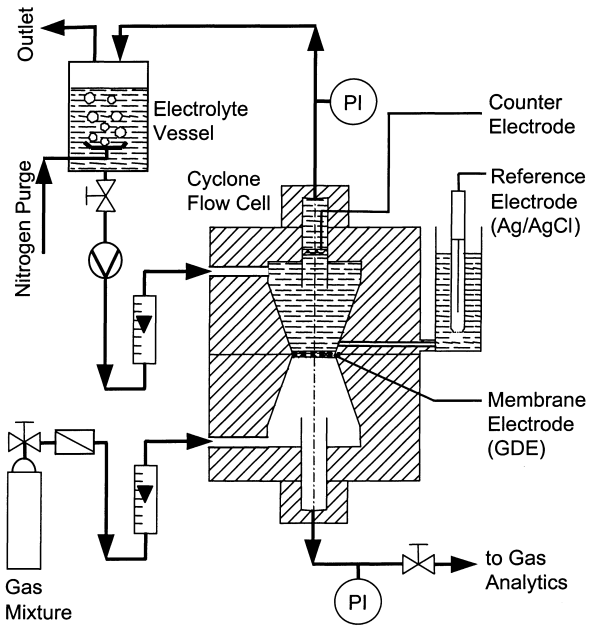

Fig. 4. Experimental set-up with cyclone flow cell.

ions. The oxidation was carried out under limiting current conditions at a nonporous graphite electrode. From the determined limiting currents, mass transfer coefficients were determined and were correlated in terms of the Sherwood number [4]

$$Sh = \frac{0.0136}{1 - t_-} Re^{2/3} Sc^{1/3} \quad (\text{for } Re > 10^3 \text{ and } Sc \geq 1) \qquad (3)$$

with the dimensionless parameter groups

$$Sh \equiv \frac{k^{\mathrm{L}} R}{D^{\mathrm{L}}} \quad (\text{Sherwood number}) \qquad (4)$$

$$Re \equiv \frac{\omega R^2 \rho}{\mu} \quad (\text{Reynolds number}) \qquad (5)$$

$$Sc \equiv \frac{\mu}{\rho D^{\mathrm{L}}} \quad (\text{Schmidt number}) \qquad (6)$$

In Eq. (3), t_- is the anion transference number. For uncharged molecules, such as chlorine, Eq. (3) is also applicable with $t_- = 0$. Thus, with the help of this equation, the mass transport coefficient through the hydrodynamic boundary layer can be calculated for any species as a function of the physico-chemical properties of the system, the geometry of the cyclone flow cell and the angular velocity of the fluid. The latter one is calculated from the fluid flow rate and the geometry. For the given geometry, the following relation is derived (for more details see [4]):

$$\omega\,(\mathrm{s}^{-1}) = 19.2 V\,(\mathrm{cm}^3\,\mathrm{s}^{-1}) \qquad (7)$$

Based on Eqs. (3)–(7), one can determine the mass transport resistance within the membrane pores of a GDE membrane from experimental data by simply substracting the external resistances from the measured total mass transport resistance. This is allowed since the roughness of the here applied graphite electrode is nearly identical similar to that of the porous membrane electrodes whose external surface is very smooth due to the production process (see Section 4). Therefore, external mass transfer towards the nonporous graphite electrode is nearly identical to external mass transfer towards the outer surface of the porous membrane electrodes which were applied for electrochemical gas absorption.

4. Membrane preparation

The feasibility of the described membrane reactor concept depends on the availability of GDE membranes whose pore structure exhibits low resistances to gas-diffusional transport and allows to stabilize the gas–liquid interface within the pores to avoid liquid breakthrough. Such GDE-membranes were produced by a calendering rolling process which is briefly outlined in the following.

The GDE membranes consist of carbon black and a polymer binder. The carbon black (Vulcan XC-72, Cabot), as the solid component, provides for the electric conductivity and the surface area on which the electrochemical reaction can take place. The polymeric binder is PTFE (Teflon®) to obtain a sufficient chemical stability and to achieve a hydrophobic surface to prevent the liquid electrolyte from flooding the whole internal pore volume.

Fig. 5 shows schematically the production process of the membranes. The carbon black and the PTFE-emulsion are mixed with water to form a paste (weight ratio: carbon black/PTFE = 70/30 wt.%). This is then dried and milled to get small, porous particles with a rubber-like surface and elasticity. These are passed through several sieves to obtain distinct particle size fractions, which are combined again in

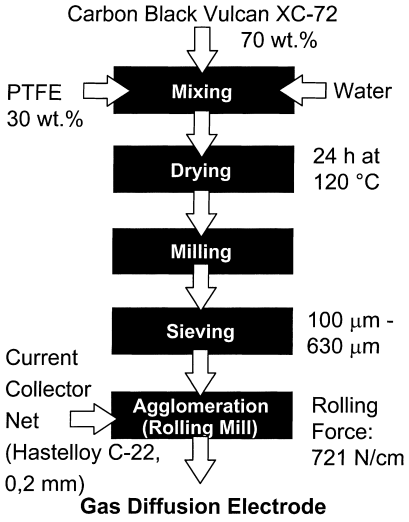

Fig. 5. Membrane production process developed by ICVT, TU Clausthal (for more details see [10–12]).

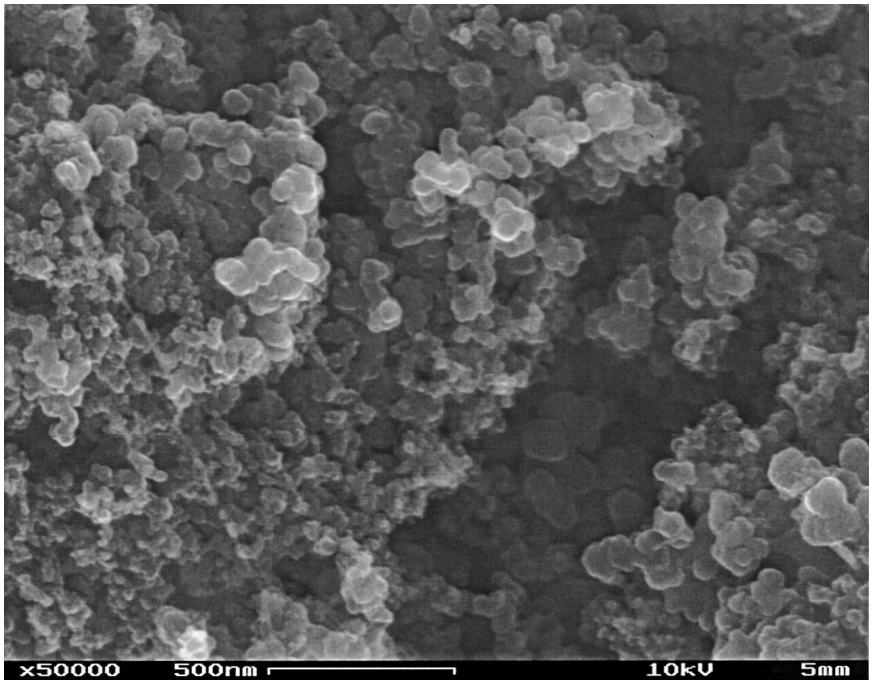

Fig. 6. SEM image of membrane pore structure (70 wt.% carbon black VULCAN XC-72/30 wt.% PTFE, rolling force 900 N cm^{-1}).

fixed ratios. Finally, the particles are pressed onto a metal net (as current collector, wire of 0.2 mm in diameter) using a calendering rolling mill. For the chlorine absorption, a special nickel alloy (Hastelloy C-22) was used for the metal net, which is highly chemically stable in the presence of chlorine and hydrochloric acid. The particles pressed onto this net form a porous agglomerate. At the applied rolling forces around 700 N cm^{-1} (force per roll length), the calendering process yields membranes with a smooth outer surface.

A more detailed description of the production process is given in [10–12]. The porous structure can be seen clearly on the SEM photograph of such a membrane (Fig. 6). The small spheres, ca. 50 nm in diameter, are the original carbon black particles which are forming agglomerates held together by PTFE.

Very important for the further understanding of the mass transport processes inside this structure is the pore volume distribution. Fig. 7 shows this distribution measured at a GDE membrane produced by calendering rolling. Obviously, the distribution is bimodal, as was expected from the production process: one finds micropores within the original carbon black particles (mean diameter 1.31 nm) and mesopores between the original carbon black particles (mean diameter 32.4 nm).

5. Electrochemical chlorine reduction experiments

The electrochemical chlorine reduction follows the overall reaction scheme:

$$Cl_2(g) + 2e^- \leftrightarrow 2Cl^-(aq); \qquad U^\theta = 1.358\,V \tag{8}$$

A series of experiments were carried out with the above described cyclone flow cell using carbon black/PTFE membranes (thickness 0.75 mm). Hydrochloric acid of 1N was circulated through the upper compartment at a flow rate of $V^L = 13.3\,cm^3\,s^{-1}$. This solution was purged with nitrogen in the external vessel shown in Fig. 4 to remove any dissolved chlorine or oxygen from the liquid bulk phase. The lower cell compartment was fed with a gas mixture containing 1000 ppm Cl_2 in N_2 (Linde).

In the first set of experiments, the influence of the gas overpressure across the membrane Δp^G on the effective current density was investigated at constant gas flow rate and constant electrode potential (Fig. 8). Above $\Delta p^G = 10$ kPa,

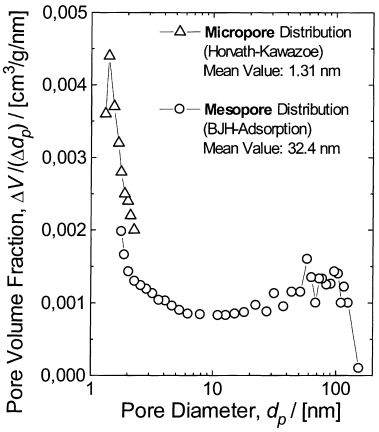

Fig. 7. Pore size distribution of used membranes (70 wt.% carbon black VULCAN XC-72/30 wt.% PTFE, rolling force 900 N cm^{-1}).

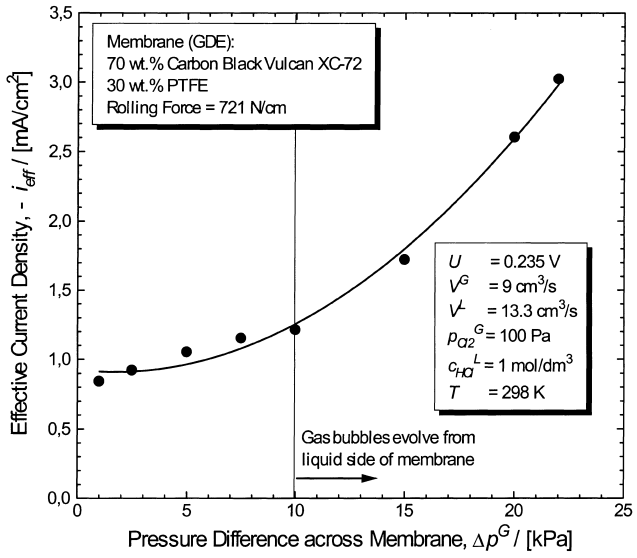

Fig. 8. Experimental current densities observed for the reduction of chlorine in hydrochloric acid versus pressure difference across membrane (measured at constant electrode potential U).

a significant increase in the current density was observed, while gas bubbles started evolving from the membrane surface. Therefore, $\Delta p^{\mathrm{G}} = 7.5\,\mathrm{kPa}$ was applied in all subsequent experiments to be sure that the transport phenomena inside the membrane pores are characterized only under conditions of a stable gas–liquid interface.

The second set of experiments was aimed at finding out about the influences of the electrode potential U and the gas flow rate V^{G} on the effective current density at a fixed gas overpressure of $\Delta p^{\mathrm{G}} = 7.5\,\mathrm{kPa}$ and variable electrode potentials U. The experimental polarization curves plotted in Fig. 9 show an increase of the absolute observable current density with increasing gas flow rate for electrode potentials

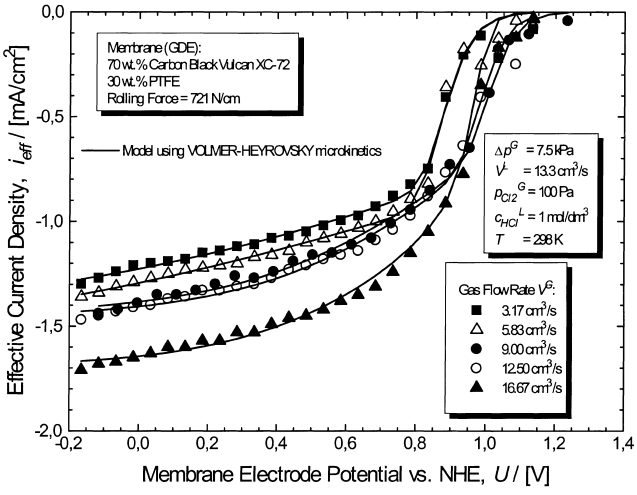

Fig. 9. Experimental and analyzed potentiostatic polarization curves for the reduction of chlorine at gas-diffusion electrode membrane; influence of gas flow rate V^{G}.

$U < 1.2\,\mathrm{V}$ (in Fig. 9, note that cathodic currents are negative by convention). From these experimental data, important physico-chemical parameters such as internal diffusion coefficients and reaction kinetic constants were estimated with the help of a macrokinetic model which is described in Section 6.

6. Model-based analysis

Many models of different complexity have been proposed to describe the operating behavior of GDE membranes. Some authors favored a quasi-homogenous (macroscopic) approach [13,14], others a heterogeneous model [15–19]. The latter often requires many adjustable parameters. Due to the limited accuracy of experimental data, some of the model parameters have little statistical significance.

Therefore, it is reasonable to follow Newman [20], and apply a macroscopic model in terms of volume-averaged quantities. The derivation of the applied steady state model for the electrochemical absorption of chlorine will be described briefly in the following. A more detailed derivation can be found in a previous paper of our group [21].

Some general assumptions have been made:

- The liquid electrolyte is not evaporating at the gas–liquid interface.
- The Ohmic drop in the electrode matrix and the electrolyte solution is negligible due to high conductivity of carbon black and hydrochloric acid, respectively. This is also justified by the fact that observed current densities are below $2\,\mathrm{mA\,cm^{-2}}$.
- Due to low chlorine concentration (<1000 ppm in gas phase), this is a highly diluted system with respect to chlorine. Therefore, it is justified to assume Fickian diffusion of chlorine in the four layers (external gas film, gas-filled electrode layer, flooded electrode layer, external liquid film).

6.1. Material balance

The mass flux densities in the non-reactive layers, i.e. in the external gas film, in the gas-filled electrode layer and in the external liquid film, are constant. In the flooded electrode layer, the mass flux density of chlorine varies according to the transfer current density per electrode volume ai_n. For the flooded layer, the following dimensionless material balance is derived:

$$\frac{\mathrm{d}^2 c^*_{\mathrm{Cl_2}}}{\mathrm{d}r^{*2}} = -(d^* Ha)^2 i_n^* \tag{9}$$

Eq. (9) is formulated in terms of some dimensionless parameter groups whose definitions and interpretations are listed in Table 1. The parameter groups are similar to those used in chemical absorption theory. However, in the considered case the rate, i.e. the local charge transfer current density $i_n{}^*$ depends on the electrode overpotential.

Table 1
Definition and interpretation of dimensionless parameter groups

Parameter	Definition	Interpretation
Spacial coordinate	$r^* \equiv \frac{r}{d^{\mathrm{FL}}}$	$\frac{\text{Spacial coordinate}}{\text{Thickness of flooded layer}}$
Hatta number	$Ha \equiv d\sqrt{\frac{ai_0/nF}{D^{\mathrm{FL}}_{\mathrm{eff},\mathrm{Cl_2}} c^{\mathrm{Le}}_{\mathrm{Cl_2}}(p^{\mathrm{G}}_{\mathrm{Cl_2}})}}$	$\frac{\text{Reaction rate under liquid bulk conditions}}{\text{Pore diffusion rate of } \mathrm{Cl_2} \text{ in flooded layer}}$
Thickness of flooded membrane layer membrane	$d^* \equiv \frac{d^{\mathrm{FL}}}{d}$	$\frac{\text{Thickness of flooded layer}}{\text{Total thickness of electrode}}$
Ratio of mass transport resistances	$D^* \equiv \frac{D^{\mathrm{FL}}_{\mathrm{eff},\mathrm{Cl_2}} c^{\mathrm{FL}}_{\mathrm{Cl_2}}(p^{\mathrm{G}}_{\mathrm{Cl_2}})}{D^{\mathrm{GL}}_{\mathrm{eff},\mathrm{Cl_2}} p^{\mathrm{G}}_{\mathrm{Cl_2}}/RT}$	$\frac{\text{Pore diffusion rate of } \mathrm{Cl_2} \text{ in flooded layer}}{\text{Pore diffusion rate of } \mathrm{Cl_2} \text{ in gas-filled layer}}$
Biot mass number for gas side	$Bi^{\mathrm{G}}_{\mathrm{m}} \equiv \frac{k^{\mathrm{G}}_{\mathrm{Cl_2}} d}{D^{\mathrm{GL}}_{\mathrm{eff},\mathrm{Cl_2}}}$	$\frac{\text{Mass transfer rate of } \mathrm{Cl_2} \text{ in gas phase}}{\text{Pore diffusion rate of } \mathrm{Cl_2} \text{ in gas-filled layer}}$
Biot mass number for liquid side	$Bi^{\mathrm{L}}_{\mathrm{m}} \equiv \frac{k^{\mathrm{L}}_{\mathrm{Cl_2}} d}{D^{\mathrm{FL}}_{\mathrm{eff},\mathrm{Cl_2}}}$	$\frac{\text{Mass transfer rate of } \mathrm{Cl_2} \text{ in liquid phase}}{\text{Pore diffusion rate of } \mathrm{Cl_2} \text{ in flooded layer}}$
Liquid bulk concentration of Cl_2	$c^*_{\mathrm{Cl_2}} \equiv \frac{c^{\mathrm{L}}_{\mathrm{Cl_2}}}{c^{\mathrm{Le}}_{\mathrm{Cl_2}}(p^{\mathrm{G}}_{\mathrm{Cl_2}})}$	$\frac{\text{Concentration of } \mathrm{Cl_2} \text{ in liquid bulk}}{\text{Equilibrium concentration of } \mathrm{Cl_2} \text{ at } p^{\mathrm{G}}_1}$
Local current density	$i^*_n \equiv \frac{i_n}{i_0(\underline{c}_{\mathrm{ref}})}$	$\frac{\text{Local current density}}{\text{Exchange current density at reference concentration}}$
Effective current density	$i^*_{\mathrm{eff}} \equiv \frac{\nu_{\mathrm{Cl_2}} i_{\mathrm{eff}} d^{\mathrm{GL}}}{nFD^{\mathrm{GL}}_{\mathrm{eff},\mathrm{Cl_2}} p^{\mathrm{G}}_{\mathrm{Cl_2}}/RT}$	$\frac{\text{Total current density}}{\text{Maximum current density}}$

For the solution of the differential equation, Eq. (9), two dimensionless boundary conditions are formulated:

$$-\left.\frac{\mathrm{d}c^*_{\mathrm{Cl_2}}}{\mathrm{d}r^*}\right|_{r^*=0} = \frac{1 - c^*_{\mathrm{Cl_2}}(r^*=0)}{(D^*/Bi^{\mathrm{G}}_{\mathrm{m}}d^*) + (D^*(1-d^*)/d^*)} \tag{10}$$

$$-\left.\frac{\mathrm{d}c^*_{\mathrm{Cl_2}}}{\mathrm{d}r^*}\right|_{r^*=1} = Bi^{\mathrm{L}}_{\mathrm{m}} d^* (c^*_{\mathrm{Cl_2}}(r^*=1) - c^{*\mathrm{L}}_{\mathrm{Cl_2}}) \tag{11}$$

The first equation gives the absorption rate at the gas–liquid interface, which is influenced by transfer resistances in the external gas film and in the gas-filled part of the electrode membrane pores. The second equation describes the leakage rate from the liquid side electrode surface towards the liquid bulk, which is controlled by external liquid film diffusion.

6.2. Reaction microkinetics

As a first kinetic approach the following Butler–Volmer type polarization equation can be used:

$$i^*_n \equiv \frac{i_n}{i_0(T, p^{\mathrm{G}}_{\mathrm{Cl_2}}, c^{\mathrm{L}}_{\mathrm{Cl^-}})} = \exp\left(\frac{\alpha_{\mathrm{a}}F}{RT}\eta\right)\left(\frac{c^{\mathrm{FL}}_{\mathrm{Cl^-}}}{c^{\mathrm{L}}_{\mathrm{Cl^-}}}\right)^2 - \exp\left(\frac{\alpha_{\mathrm{c}}F}{RT}\eta\right)\left(\frac{c^{\mathrm{FL}}_{\mathrm{Cl_2}}}{c^{\mathrm{Le}}_{\mathrm{Cl_2}}(p^{\mathrm{G}}_{\mathrm{Cl_2}})}\right) \tag{12}$$

Although Eq. (12) is very popular in electrochemical engineering, it is important to mention that this rate law is an adequate approach for single elementary reactions only, i.e. for a single electron transfer. However, the electrochemical chlorine reduction consists of more than one elementary reaction step. Therefore, a more reasonable rate approach should be based on multi-step reaction mechanisms, such as Volmer–Tafel or Volmer–Heyrovsky (see e.g. [22]). A thorough comparison of the different possible reaction mechanisms with the experimental results was carried out. For lack of space, this comparison is not given in full detail, instead we directly report the outcome of this analysis: for chlorine reduction at carbon black electrode material, the Volmer–Heyrovsky mechanism was found to be the adequate one:

$$\mathrm{Cl_2(g)} + \mathrm{e^-} + \mathrm{S} \rightarrow \mathrm{Cl^{\bullet}S} + \mathrm{Cl^-(aq)}$$

Heyrovsky reaction (13)

$$\mathrm{Cl^{\bullet}S} + \mathrm{e^-} \leftrightarrow \mathrm{Cl^-(aq)} + \mathrm{S}$$

Volmer reaction (14)

S denotes a free adsorption site on the electrode surface. In the first step, the Heyrovsky reaction, soluted chlorine adsorbes at the electrode surface accompanied by transfer of one electron. By this, an adsorbed chlorine radical ($Cl^{\bullet}S$) and a chloride ion are formed. In the second step, the Volmer reaction Eq. (14), another electron is transferred to the adsorbed chloride radical forming a second chloride ion.

The Heyrovsky reaction is assumed to be rate determining. The rate constant of the anodic Heyrovsky reaction is

denoted as $k_{a,H}$, the rate constant of the cathodic reaction is denoted as $k_{c,H}$. For the local current density i_n of the Heyrovsky reaction, the following expression for the charge transfer current density is formulated:

$$\frac{i_n}{n_H F} = k_{a,H}(T)\exp\left\{\frac{(1-\beta_{S,H})n_H F}{RT}(\phi^S-\phi^{FL})\right\}\Theta_{Cl}a^{FL}_{Cl^-} - k_{c,H}(T)\exp\left\{-\frac{\beta_{S,H}n_H F}{RT}(\phi^S-\phi^{FL})\right\}\Theta_S a^{FL}_{Cl_2} \quad (15)$$

The rate constant of the anodic Volmer reaction be $k_{a,V}$ and that of the corresponding cathodic reaction be $k_{c,V}$. As the Volmer reaction is assumed to be fast in comparison to the Heyrovsky reaction step, it is close to equilibrium. This yields

$$k_{a,V}(T)\exp\left\{\frac{(1-\beta_{S,V})n_V F}{RT}(\phi^S-\phi^{FL})\right\}\Theta_S a^{FL}_{Cl^-} = k_{c,V}(T)\exp\left\{-\frac{\beta_{S,V}n_V F}{RT}(\phi^S-\phi^{FL})\right\}\Theta_{Cl} \quad (16)$$

From Eq. (16) one obtains

$$\frac{\Theta_S a^{FL}_{Cl^-}}{\Theta_{Cl}} = K_V(T,\phi^S-\phi^{FL}) \quad (17)$$

with K_V as temperature dependent and potential dependent equilibrium constant of the Volmer reaction:

$$K_V \equiv \frac{k_{c,V}(T)}{k_{a,V}(T)}\exp\left\{-\frac{F}{RT}(\phi^S-\phi^{FL})\right\} \quad (18)$$

As long as only chlorine radicals adsorb at the surface, the balance for the surface fractions is given by

$$\Theta_{Cl}+\Theta_S = 1 \quad (19)$$

Inserting this into Eq. (17), one gets the surface fractions

$$\Theta_{Cl} = \frac{a^{FL}_{Cl^-}/K_V}{1+(a^{FL}_{Cl^-}/K_V)} \quad (20)$$

and

$$\Theta_S = \frac{1}{1+(a^{FL}_{Cl^-}/K_V)} \quad (21)$$

Because of Eq. (18), the surface fraction depends on the difference between the electrostatic potentials of the solid and the electrolyte solution (liquid phase). Inserting the surface fraction of chlorine into the rate expression of the Heyrovsky reaction (Eq. (15)) leads to an expression for the transfer current density in terms of the liquid phase activities a_i:

$$i_n = Fk_{a,H}(T)\exp\left\{\frac{(1-\beta_{S,H})F}{RT}(\phi^S-\phi^{FL})\right\}\times\frac{(a^{FL}_{Cl^-})^2/K_V}{1+(a^{FL}_{Cl^-}/K_V)} - Fk_{c,H}(T)\times\exp\left\{-\frac{\beta_{S,H}F}{RT}(\phi^S-\phi^{FL})\right\}\frac{a^{FL}_{Cl_2}}{1+(a^{FL}_{Cl^-}/K_V)} \quad (22)$$

The current density i_n equals zero in the electrochemical equilibrium. Then, the potential difference between solid and liquid phase, taking into account the potential dependence of the Volmer equilibrium constant K_V (Eq. (18)), is given by

$$(\phi^S-\phi^{FL})_{i_n=0} = \frac{RT}{2F}\ln\left(\frac{k_{c,H}}{k_{a,H}}\frac{k_{c,V}}{k_{a,V}}\frac{a^{FL}_{Cl_2}}{(a^{FL}_{Cl^-})^2}\right) \quad (23)$$

The exchange current density i_0 is defined as

$$i_0 \equiv Fk_{a,H}(T)\exp\left\{\frac{(1-\beta_{S,H})F}{RT}(\phi^S-\phi^{FL})_{i_n=0}\right\}\times\frac{(a^{L}_{Cl^-})^2}{K_V(T,(\phi^S-\phi^{FL})_{i_n=0})} = Fk_{c,H}(T)\times\exp\left\{-\frac{\beta_{S,H}F}{RT}(\phi^S-\phi^{FL})_{i_n=0}\right\}a^{Le}_{Cl_2} \quad (24)$$

With Eqs. (23) and (24), the reaction rate expression can be formulated in terms of the overpotential

$$\eta \equiv (\phi^S-\phi^{FL}) - (\phi^S-\phi^{FL})_{i_n=0,a^{Le}_{Cl_2},a^{L}_{Cl^-}} \quad (25)$$

Neglecting the non-ideal mixing behavior in the reaction mixture, one can substitute activities by molar concentrations. This yields the following expression for the charge transfer current density

$$i_n = i_0(T,p^G_{Cl_2},c^L_{Cl^-})\times\frac{\exp\{(\alpha_{a,H}F/RT)\eta\}(c^{FL}_{Cl^-}/c^{L}_{Cl^-})^2 - \exp\{(-\alpha_{c,H}F/RT)\eta\}(c^{FL}_{Cl_2}/(c^{Le}_{Cl_2}(p^G_{Cl_2})))}{1+(c^{FL}_{Cl^-}/c^{L}_{Cl^-})(a^{L}_{Cl^-}/K_{V,0}(T))\exp\{(F/RT)\eta\}} \quad (26)$$

This expression contains not only the kinetic parameters, i.e. the exchange current density i_0 and the anodic and the cathodic charge transfer coefficients

$$\alpha_{a,H} \equiv 2-\beta_{S,H} \quad (27)$$

and

$$\alpha_{c,H} \equiv \beta_{S,H} \quad (28)$$

but also the equilibrium constant of the Volmer reaction, $K_{V,0}$, at the potential difference in the electrochemical equilibrium:

$$K_{V,0}(T) \equiv \frac{k_{c,V}(T)}{k_{a,V}(T)}\exp\left\{-\frac{F}{RT}(\phi^S-\phi^{FL})_{i_n=0}\right\} \quad (29)$$

From Eq. (26) one can see, that the Volmer–Heyrovsky mechanism leads to a rate expression, that is of first-order

with respect to chlorine, as long as the Heyrovsky reaction is rate determining. On the other hand, the dependence of the current density on the chloride ion concentration does not follow a power law.

For the analysis, it is adequate to work with a high chloride concentration compared to the chlorine concentration. This was achieved in the experiments by using a 1N solution of hydrochloric acid as the liquid electrolyte phase, i.e. $c^{\mathrm{FL}}_{\mathrm{Cl}^-} = c^{\mathrm{L}}_{\mathrm{Cl}^-} = 1\,\mathrm{mol\,dm^{-3}}$. The reference activity of the chloride ions, i.e. their activity in the liquid bulk, is approximated by $a^{\mathrm{L}}_{\mathrm{Cl}^-} = 1$. The rate expression, Eq. (26), then simplifies to give the following dimensionless rate expression

$$i_n^* \equiv \frac{i_n}{i_0(T, p^{\mathrm{G}}_{\mathrm{Cl}_2}, c^{\mathrm{L}}_{\mathrm{Cl}^-})} = \frac{\exp\{(\alpha_{\mathrm{a,H}}F/RT)\eta\} - \exp\{(-\alpha_{\mathrm{c,H}}F/RT)\eta\}(c^{\mathrm{FL}}_{\mathrm{Cl}_2}/(c^{\mathrm{Le}}_{\mathrm{Cl}_2}(p^{\mathrm{G}}_{\mathrm{Cl}_2})))}{1 + (1/K_{\mathrm{V},0}(T))\exp\{(F/RT)\eta\}} \tag{30}$$

For $K_{\mathrm{V},0} \to \infty$, i.e. negligible adsorption of chlorine radicals, this rate expression becomes identical to the Butler–Volmer approach, Eq. (12). To identify the Volmer constant $K_{\mathrm{V},0}$, one has to know the dependence of the local current density i_n on the electrode overpotential η, i.e. the reaction microkinetics. However, the only observable current density is the global current density i_{eff} at the total electrode surface, i.e. the reaction macrokinetics, which also depends on mass transport effects.

6.3. Reaction macrokinetics

The combination of the mass balance, Eq. (9), with the rate expression, Eq. (30), yields a linear differential equation for the chlorine concentration profile $c^*_{\mathrm{Cl}_2}(r^*)$ which can be solved analytically [21]. From this solution, the chlorine absorption and leakage rates on both sides of electrode, Eqs. (10) and (11), are determined. With the help of this, the observable, effective current density i^*_{eff} is calculated as follows:

$$i^*_{\mathrm{eff}} \equiv \frac{i_{\mathrm{eff}}}{i_{\max}} = D^* \frac{1-d^*}{d^*} \left(- \left.\frac{\mathrm{d}c^*_{\mathrm{Cl}_2}}{\mathrm{d}r^*}\right|_{r^*=0} + \left.\frac{\mathrm{d}c^*_{\mathrm{Cl}_2}}{\mathrm{d}r^*}\right|_{r^*=1} \right) \tag{31}$$

Eq. (31) is based on an overall chlorine balance across the membrane, i.e. the total electrochemical conversion of chlorine is proportional to the difference of chlorine absorption rate (first differential in brackets) and the chlorine leakage rate (second differential in brackets). In Eq. (31), the effective current density i_{eff} is related to the maximum current density $i_{\max}$. This maximum value will be observed if only the mass transport resistance in the gas-filled membrane layer dominates the electrochemical conversion. Using Faraday's law, the maximum current density is calculated from

$$i_{\max} = nF \frac{D^{\mathrm{GL}}_{\mathrm{eff,Cl}_2}}{d^{\mathrm{GL}}} \frac{p^{\mathrm{G}}_{\mathrm{Cl}_2}}{RT} \tag{32}$$

where in case of chlorine reduction, the number of transferred electrons is $n = 2$. Combining Eq. (32) with the analytical solution of the concentration profile [21] yields the dimensionless observable current density

$$i^*_{\mathrm{eff}} = \frac{1}{(1/i^*_{\mathrm{lim}}) + \{D^*(1-d^*)Ha[(\exp\{-(\alpha_{\mathrm{c,H}}F/RT)\eta\}/(1 + (1/K_{\mathrm{V},0})\exp\{(F/RT)\eta\})]^{1/2}\}^{-1}} \tag{33}$$

Eq. (33) is valid for

$$\widetilde{H}a_{\mathrm{H}} = d^* Ha \sqrt{\frac{\exp\{-(\alpha_{\mathrm{c,H}}F/RT)\eta\}}{1 + (1/K_{\mathrm{V},0}(T))\exp\{(F/RT)\eta\}}} > 3 \quad \text{and} \quad \exp(n\eta^*) \to 0 \tag{34}$$

i.e. for moderately fast reaction up to instantaneous reaction. In the latter case, the reactant chlorine is totally consumed at the gas–liquid interface and its concentration there drops to zero. Then, the flooded layer resistance has no importance because the gas no longer enters the flooded layer. The resulting current density reaches the limiting current density i^*_{lim}

$$i^*_{\mathrm{lim}} = \frac{1}{1 + (1/Bi^{\mathrm{G}}_{\mathrm{m}}(1-d^*))} \tag{35}$$

Obviously, the limiting current density depends on the thickness of the gas-filled membrane layer $(1 - d^*)$, and on the gas side external mass transfer resistance, $1/Bi^{\mathrm{G}}_{\mathrm{m}}$.

In Fig. 10, the dependence of the effective current density on the electrode overpotential is depicted under variation of

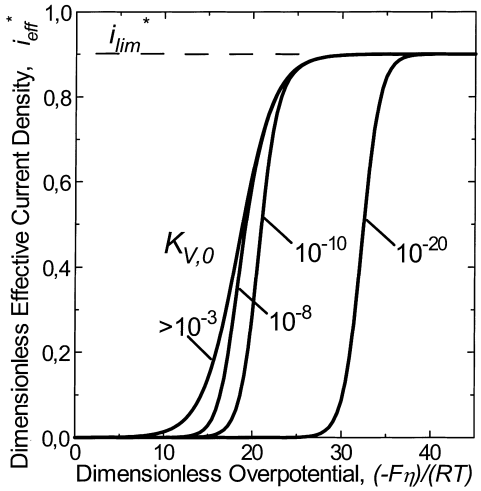

Fig. 10. Simulated dependence of effective current density on electrode overpotential for Volmer–Heyrovsky reaction mechanism under variation of Volmer reaction equilibrium constant $K_{\mathrm{V},0}$ ($Bi^{\mathrm{G}}_{\mathrm{m}} = 10$, $a_{\mathrm{c,H}} = 1$, $Ha = 10$, $d^* = 0.1$, $D^* = 10^{-5}$).

Table 2
Model parameters for chlorine reduction at gas-diffusion electrode membrane, identified by nonlinear least squares fit, for different gas flow rates[a]

Parameter	V^G ($cm^3\,s^{-1}$)				
	3.17	5.83	9.00	12.50	16.67
$-1/i_{lim}$ ($cm^2\,mA^{-1}$)	0.67 ± 0.25	0.59 ± 0.35	0.69 ± 0.04	0.68 ± 0.04	0.58 ± 0.02
$-B^b$ ($cm^2\,mA^{-1}$)	0.92 ± 0.40	0.77 ± 0.18	1.69 ± 0.66	1.70 ± 0.82	1.30 ± 0.42
$1/K_{V,0}$ ($\times 10^{-6}$)	9.54 ± 7.19	12.75 ± 10.61	0.05 ± 0.04	0.12 ± 0.11	0.33 ± 0.17
$\alpha_{c,H}$	0.08 ± 0.08	0.06 ± 0.08	0.16 ± 0.05	0.17 ± 0.06	0.17 ± 0.04

[a] Given confidence intervals are valid for a confidence number of 95%.
[b] Definition of B according to Eq. (37).

the Volmer reaction equilibrium constant, $K_{V,0}$. Evidently, at low overpotentials decreasing the Volmer constant, i.e. increasing the influence of chlorine radicals adsorption, leads to significantly lower currents. By applying higher overpotentials, the reaction is accelerated, the adsorption effect is overcome, and then the different polarization curves are approaching to one another. For very high overpotentials, the reaction is instantaneous and the limiting current i^*_{lim} is achieved.

6.4. Parameter identification

The model parameters of the macrokinetic rate expression, Eq. (33), are identified from the experimental data presented in Fig. 9. By rearranging this equation, it is easily shown that the polarization curves depend on four parameters or parameter groups, respectively.

- The reciprocal limiting current density:

$$\frac{1}{i_{lim}} = \frac{1}{i_{max}}\left(1 + \frac{1}{Bi^G_m(1-d^*)}\right) \tag{36}$$

- The parameter group:

$$B \equiv \frac{1}{i_{max}D^*(1-d^*)}Ha \tag{37}$$

- The reciprocal equilibrium constant of the Volmer reaction: $(1/K_{V,0})$
- The cathodic charge transfer coefficient of the Heyrovsky reaction $\alpha_{c,H}$.

To obtain these parameters, a nonlinear regression based on the Marquardt–Levenberg algorithm was applied to the experimental data. The resulting values are presented in Table 2 along with the corresponding confidence intervals. From the reciprocal value of the limiting current density i_{lim}, Eq. (36), the internal diffusion coefficient of chlorine in the gas-filled membrane layer is estimated. With $d^{GL} \approx d$, i.e. the electrode pore system is nearly totally filled with gas (which corresponds to the experimental conditions), one obtains

$$D^{GL}_{eff,Cl_2} = d\frac{i_{lim}/2F}{-(p^G_{Cl_2}/RT) - ((i_{lim}/2F)/k^G_{Cl_2})} \tag{38a}$$

From the effective diffusivity in Eq. (38), the intrinsic chlorine diffusivity $D^{GL}_{Cl_2}$ is estimated using the following correlation proposed by Newman [20]:

$$D^{GL}_{Cl_2} = \frac{D^{GL}_{eff,Cl_2}}{\varepsilon^{1.5}} \tag{38b}$$

with ε being the total porosity of the GDE membrane. The mass transport coefficient $k^G_{Cl_2}$ can be calculated with the

Table 3
Physicochemical parameters calculated from model parameters listed in Table 2 (assumption: $d^{GL} \approx d$, i.e. membrane pores nearly totally filled with gas)[a]

Parameter	V^G ($cm^3\,s^{-1}$)				
	3.17	5.83	9.00	12.50	16.67
Re^G	259	478	737	1020	1370
$k^G_{Cl_2}$ ($m\,s^{-1}$)	1.2×10^{-3}	1.8×10^{-3}	2.4×10^{-3}	3.0×10^{-3b}	3.6×10^{-3b}
$D^{GL}_{Cl_2}$ ($10^{-7}\,m^2\,s^{-1}$)	4.85	5.26	4.28	4.11	5.01
i_{max} ($mA\,cm^{-2}$)	1.78	1.93	1.57	1.57	1.84
ai_0 ($A\,m^{-3}$)	81.9×10^{-3}	116.9×10^{-3}	24.3×10^{-3}	24.0×10^{-3}	41.0×10^{-3}
$d_{p,eq}$ (nm)[c]	4.9	5.3	4.3	4.3	5.0

[a] Additional physical properties: electrode thickness $d = 0.75$ mm; overall porosity of electrode $\varepsilon = 0.5$; partial pressure of chlorine in the gas bulk $p^G_{Cl_2} = 10^2$ Pa; chlorine concentration at $c^L_{Cl_2}(p^G_{Cl_2}) = 0.573\,mol\,m^{-3}$; gas-phase diffusion coefficient of chlorine in a mixture with nitrogen $D^G_{Cl_2,N_2} = 1.85 \times 10^{-5}\,m^2\,s^{-1}$ (estimated using the Wilke–Lee correlation [23]); liquid-phase diffusion coefficient of chlorine at infinite dilution in water $D^{L,\infty}_{Cl_2,H_2O} = 3.69 \times 10^{-10}\,m^2\,s^{-1}$ (estimated using the Wilke–Chang correlation [24]); molecular weight of chlorine $M_{Cl_2} = 0.0709\,kg\,mol^{-1}$.
[b] Sherwood function, Eq. (3), extrapolated.
[c] Pore equivalent diameter calculated from Eq. (40).

help of the cyclone cell Sherwood function, Eq. (7). For Reynolds numbers, Re^{G}, between 260 and 1400, one obtains values of $k^{G}_{Cl_2}$ from 1×10^{-3} to $4\times10^{-3}\,m\,s^{-1}$ (see Table 3).

From the values of the parameter group B, the exchange current density related to the electrode volume ai_0 is estimated:

$$ai_0 = \frac{1}{2FD^{GL}_{eff,Cl_2}c^{Le}_{Cl_2}B^2} \tag{39}$$

The results of the analysis based on Eqs. (38) and (39) can be found in Table 3.

From the internal diffusion coefficient of chlorine, $D^{GL}_{Cl_2}$ (Eq. (38b)), one can estimate the mean pore size of the membrane. Due to the fact, that the experimentally determined pore size distribution is between 1 and 100 nm (see Fig. 7), chlorine diffusion is expected to take place in the Knudsen regime. Therefore, the pore equivalent diameters $d_{p,eq}$ are calculated from the Knudsen diffusivity formula as follows:

$$d_{p,eq} = \frac{3}{2}D^{GL}_{Cl_2}\sqrt{\frac{\pi}{2}\frac{M_{Cl_2}}{RT}} \tag{40}$$

The results are given in Table 3.

7. Discussion

In general, the comparison between experimental and analyzed results (Fig. 9) shows a good agreement. It is important to mention that all identified model parameter values are statistically significant as indicated by the confidence intervals listed in Table 2. Thus, the derived model is adequate to describe the steady state behavior of the electrochemical chlorine absorption at a GDE membrane.

Fig. 11 shows a selected experimental polarization curve at a gas flow rate of $V_G = 16.67\,cm^3\,s^{-1}$. The fine dotted line in Fig. 11 reveals that experimental results are not properly matched by the Butler–Volmer approach. This is due to the fact that the Butler–Volmer rate expression is only valid for single elementary reactions, e.g. a single electron transfer, while the electrochemical chlorine reduction consists of more than one elementary reaction step. The bold line in Fig. 11, shows the result of a model fit using the Volmer–Heyrovsky rate expression, Eq. (30). Here, a good agreement with the experimental data is attained. Obviously, the adsorption of chlorine radicals significantly influences the overall reaction kinetics. This is confirmed by the equilibrium constants of the Volmer reaction determined from the experimental data. They are in the region of $K_{V,0} = 10^{-6}$. Thus, the inner electrode surface sites are nearly totally occupied by adsorbed chlorine radicals, i.e. $\Theta_{Cl} \approx 1$.

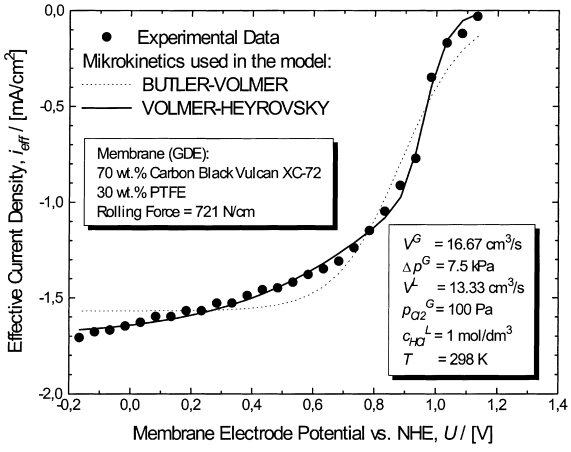

Fig. 11. Experimental and analyzed potentiostatic polarization curves for the reduction of chlorine at gas-diffusion electrode membrane.

The determined diffusion coefficients of chlorine in the gas-filled pore volume in the membrane are located in the Knudsen diffusion regime (see Table 3). The estimated pore equivalent diameters, $d_{p,eq}$, ranges from 4.3 to 5.3 nm. By comparison with the experimental pore size distribution (Fig. 7), one can conclude that gas transport in the membrane is dominated mainly by micropore diffusion, i.e. diffusion within the pores which are in the carbon black precursors.

The calculated charge transfer coefficients of the Heyrovsky reaction are quite low. They are around $\alpha_{c,H} < 0.18$ which leads to the presumption that the electrochemical reaction is inhibited by additional diffusional resistances, which are not implemented adequately in the actual model. For this reason, in the literature some authors favor the flooded-agglomerate model [15–19]. It accounts for the bimodality of the pore diameter distribution of a GDE. With this model, it may be shown that the combination of diffusional resistances in the micro- and the macropores leads to considerably lower, effective charge transfer coefficients.

8. Conclusions

Based on the experimental and theoretical results presented above, the following conclusions can be drawn:

- The proposed electrochemical gas–liquid membrane absorber is a feasible reactor concept, especially for the purification of waste gas streams containing very low contents of pollutants which are electrochemically convertable.
- The reactor principle is based on dispersionless contacting of gas and liquid phases within the pore structure of electrically conductive membranes. By increasing the absolute membrane electrode overpotential, the rate of electrochemical reaction can be varied in a wide range from slow reaction up to instantaneous regime.
- At instantaneous conditions, the absorption rate is limited mainly by mass transfer resistances in the gas-filled micropores of the electrode membrane layer. This is in contrast to classical gas–liquid countercurrent fixed bed absorbers whose performance is dominated by liquid film diffusion. Therefore, for the membrane reactor concept to

achieve better performance than a classical fixed absorber, it is decisive that the membrane thickness is small enough (below 0.5 mm). On the other hand, a minimum thickness is needed to attain a reasonable mechanical stability of the membrane. As a consequence for further research one should apply supported asymmetric membranes with a thin gas–liquid contacting layer on top.

- It turned out that diffusion coefficients in the porous membrane can be estimated very efficiently from potentiostatic polarization curves measured under well defined vortex flow fields in a novel cyclone type reactor.
- Under slow and fast reaction conditions, the chlorine absorption rate is decreased by strong adsorption of chlorine radicals on the inner surface of the carbon black electrode material.
- Based on systematic experiments in the cyclone reactor, a validated model for the electrochemical absorption macrokinetics was established. With the help of this model, it is now possible to design large scale membrane absorbers for the purification of waste gases.

Acknowledgements

The authors wish to thank Prof. Ulrich Hoffmann, Institut für Chemische Verfahrenstechnik at the Technical University of Clausthal, for supporting this research work in his labs during our time there. We are also grateful to Prof. Gerhard Emig and coworkers, Institut für Technische Chemie at the University of Erlangen-Nürnberg, for carrying out the pore size measurements.

References

[1] G. Kreysa, K. Jüttner, Towards a cleaner environment using electrochemical techniques, in: F. Lapicque, A. Storck, A. Wragg (Eds.), Electrochemical Engineering and Energy, Plenum Press, New York, 1995, pp. 255–270.
[2] K. Sundmacher, Reaktionstechnische Grundlagen der elektrochemischen Absorption mit Gasdiffusionselektroden, VDI-Fortschrittsbericht No. 564, VDI-Verlag, Düsseldorf, 1998.
[3] B. Elvers, S. Hawkins, W. Russey, G. Schulz (Eds.), Ullmann's Encyclopedia of Industrial Chemistry, 5th Edition, Vol. A23, VCH Verlagsgesellschaft, Weinheim, 1991, pp. 635–642.
[4] K. Sundmacher, Cyclone flow cell for the investigation of gas-diffusion electrodes, J. Appl. Electrochem. 29 (1999) 919–926.
[5] G. Kreysa, H.J. Külps, Ein elektrochemisches Absorptionsverfahren zur Gasreinigung, Chem.-Ing.-Tech. 55 (1983) 55–59.
[6] K. Sundmacher, U. Hoffmann, Design and operation of a membrane reactor for electrochemical gas purification, Chem. Eng. Sci. 54 (1999) 2937–2945.
[7] H. Schlichting, Boundary-Layer Theory, 7th Edition, McGraw-Hill, New York, 1987.
[8] U.T. Bödewadt, ZAMM 20 (1940) 241–253.
[9] J.E. Nydahl, Heat transfer for the BÖDEWADT problem, Dissertation, Colorado State University, Fort Collins, 1971.
[10] R. Hamelmann, K. Sundmacher, U. Hoffmann, Einsatz eines Kalanderwalzwerkes zur reproduzierbaren Herstellung von porösen Elektroden auf Kohlenstoffbasis, GdCH Jahrestagung der Fachgruppe Angewandte Elektrochemie, Monheim, 9–12 October 1996.
[11] O. Nowitzki, R. Hamelmann, K. Sundmacher, U. Hoffmann, Production of gas-diffusion-electrodes loaded with non-noble metal catalyst for oxygen reduction by a calendering rolling process, in: I. Rousar (Ed.), Contemporary Trends in Electrochemical Engineering, UTAX, Prague, 1996, pp. 227–233.
[12] H. Fasse, Verfahrenstechnischer Beitrag zur Elektrodenherstellung für Brennstoffzellen, Dissertation, TU Clausthal, 1997.
[13] D.M. Bernardi, M.W. Verbrügge, Mathematical model of a gas diffusion electrode bonded to a polymer electrolyte, AIChE J. 37 (1991) 1151–1163.
[14] T.E. Springer, M.S. Wilson, S. Gottesfeld, Modeling and experimental diagnostics in polymer electrolyte fuel cells, J. Electrochem. Soc. 140 (1993) 3513–3526.
[15] R.P. Iszkowski, M.B. Ncutlip, Voltage losses in fuel cell cathodes, J. Electrochem. Soc. 127 (1980) 1433–1440.
[16] P. Björnbom, Modeling a double-layered PTFE-bonded oxygen electrode, Electrochim. Acta 32 (1987) 115.
[17] S.J. Ridge, R.E. White, Y. Tsou, R.N. Beaver, G.A. Eisman, Oxygen reduction in a proton exchange membrane test cell, J. Electrochem. Soc. 136 (1989) 1902–1909.
[18] M.A. Al-Saleh, S. Gultekin, S. Rahman, A. Al-Zakri, Modified flooded spherical agglomerate model for gas-diffusion electrodes in alkaline fuel cells, J. Power Sources 55 (1995) 33–39.
[19] K. Broka, P. Ekdunge, Modelling of PEM fuel cell cathode, J. Appl. Electrochem. 27 (1997) 281.
[20] J.S. Newman, Electrochemical Systems, 2nd Edition, Prentice-Hall, Englewood Cliffs, NJ, 1991.
[21] K. Sundmacher, U. Hoffmann, Macroscopic analysis of polarization characteristics of gas-diffusion electrodes in contact with liquid electrolytes. Part I. First order reactions, J. Appl. Electrochem. 28 (1998) 359–368.
[22] W. Schmickler, Interfacial Electrochemistry, Oxford University Press, New York, 1996.
[23] R.C. Reid, J.M. Prausnitz, B.E. Poling, The Properties of Gases and Liquids, 4th Edition, McGraw-Hill, New York, 1987, p. 587.
[24] R.C. Reid, J.M. Prausnitz, B.E. Poling, The Properties of Gases and Liquids, 4th Edition, McGraw-Hill, New York, 1987, pp. 598–600.